

# Simultaneous shape and topology optimization of prestressed concrete beams

Oded Amir · Emad Shakour

Received: date / Accepted: date

**Abstract** This paper presents a new optimization approach for the design of prestressed concrete beams. The prestressing tendon is modeled as a chain of linear segments that transfer point forces to the concrete domain according to the tendon's angles. The concrete beam is modeled as a discretized continuum following density-based approaches to topology optimization. The shape of the tendon and the topology of the surrounding concrete are optimized simultaneously within a single problem formulation. A special filtering technique is developed in order to ensure that the tendon is covered by concrete, thus shape and topological variables are tightly coupled. Several test cases demonstrate the applicability of the proposed optimization procedure. The deformation of the optimized designs due to external loads is counteracted by the deformation due to prestressing, hence by tuning the force in the tendon the total deformation can approach zero. Consequently, the beams exhibit a compression-only response meaning that the common goal of prestressed concrete design is achieved.

**Keywords** Topology Optimization · Shape Optimization · Prestressed Concrete · Equivalent Load Method

The authors gratefully acknowledge funding received from the European Commission Research Executive Agency, grant agreement PCIG12-GA-2012-333647

O. Amir  
Faculty of Civil and Environmental Engineering, Technion – Israel Institute of Technology  
Tel.: +972-4-8293041  
E-mail: odedamir@technion.ac.il

E. Shakour  
Faculty of Civil and Environmental Engineering, Technion – Israel Institute of Technology  
E-mail: semad@campus.technion.ac.il

## 1 Introduction

Topology optimization of continuum structures is a computational methodology for optimizing the distribution of material in a given design domain. Various mathematical formulations and numerical approaches have been suggested throughout the last three decades since the method was conceived by Bendsøe and Kikuchi (1988). Early developments focusing on the density-based approach are reviewed in the monograph by Bendsøe and Sigmund (2003), whereas later developments and comparisons of different approaches can be found in recent review articles (Sigmund and Maute 2013; Deaton and Grandhi 2014). The maturity of topology optimization is reflected by its increasing utilization in industry. Particularly, the automotive and aerospace industries use it extensively for reducing weight and increasing stiffness, among other goals (Sigmund and Bendsøe 2004; Zhu et al 2015). At the same time, topology optimization has made only minor impact on traditional structural engineering as practiced in the construction industry. Examining the specific case of concrete structures, the cost of manufacturing complex forms and the difficulty in combining numerical optimization tools with accurate constitutive models are the main barriers that need to be overcome. Despite these challenges, optimizing concrete structures is of great importance because concrete is the most widely used material (besides water) and its production is a major contributor to CO<sub>2</sub> emissions (Mahasenan et al 2003; Flower and Sanjayan 2007; World Business Council for Sustainable Development 2012; Stocker et al 2013). The purpose of this paper is to present a new, simple yet effective approach for topology optimization of concrete beams that are prestressed into a compressive state using steel tendons.

Early contributions relating continuum topology optimization procedures to concrete design have focused on the automatic generation of strut-and-tie models, for example

Liang et al (2000), Liang et al (2001) and Bruggi (2009). While initially a linear-elastic material model was considered by most authors, more elaborate constitutive relations have been incorporated in recent publications, capturing the asymmetric response of concrete to tension and compression. Furthermore, these studies shifted the focus to designing the structure itself, rather than only generating its strut-and-tie model for analysis. Some studies pose the problem as a material distribution in a continuum domain, for example Liu and Qiao (2011), Victoria et al (2011), Bogomolny and Amir (2012), Luo and Kang (2012) and Luo et al (2015). Another class of formulations combines a more realistic simultaneous optimization of concrete as a continuum and reinforcement that is modeled as additional discrete (or truss-like) members, see for example Gaynor et al (2012), Amir (2013), Yang et al (2014) and Bruggi (2016). As the current contribution involves the shape optimization of steel embedded in concrete, it is worthy to mention also the work by Kato and Ramm (2010) on shape optimization of reinforcement fibers within a concrete structure.

The topic of prestressed concrete, and specifically the optimization of tendon geometry, has received only little attention. The magnitude of tendon forces, the tendon geometry and the cross-sectional dimensions were optimized assuming linear-elastic response by linear programming in the early studies by Kirsch (1972, 1973). Cohn and Lounis (1993) extended the capability of such design procedures to comply with both ultimate and serviceability limit states based on nonlinear analysis of the beams. Another interesting approach to optimizing the tendon geometry within a fixed concrete domain is based on the concept of configurational forces (Eurviryanukul and Askes 2010, 2011).

In contrast to the contributions mentioned above, the present paper aims at optimizing simultaneously both the tendon geometry and the surrounding concrete topology. This is achieved by modeling the effect of prestressing by means of the equivalent load method (Moorman 1952). The spatial coordinates of the tendon are subsequently treated as design variables, alongside the density distribution of the concrete continuum. A special filtering technique is developed in order to guarantee that the tendon is properly covered by concrete, introducing a strong coupling between shape and topological variables. The filter developed herein is inspired by a previous steel-concrete filter that was formulated for ensuring concrete cover over steel reinforcement bars in topology optimization of reinforced concrete (Amir 2013). Because the aim is to design prestressed members that do not exhibit inelastic response, linear-elastic modeling of the concrete is possible and the overall computational procedure can be executed with limited computational resources. This is an advantage compared to procedures that require either nonlinear finite element analysis or involve a large number of response constraints. As the tendon can take

any desired shape under certain restrictions on its lower and upper bounds, the methodology is applicable only to post-tensioning systems, where a duct is positioned before the concrete is cast and the tendon is inserted and tensioned after the concrete has developed sufficient strength. In contrast, pre-tensioning systems use straight tendons so there is no room for optimizing the geometry.

Ultimately, the filtering operation that couples topological and shape variables leads to a formulation that is strongly related to simultaneous approaches studied previously. In the context of design-dependent loads, Du and Olhoff (2004) generated the pressure load on the boundary of an evolving topology using isolines of the density distribution. Lee and Martins (2012) extended this approach using prescribed initial void regions leading to the applicability in the case of multiple pressure vessels. Another related approach was presented by Zhu et al (2008) who coupled the optimization of component locations and the layout of their supporting structure. Conceptually, this approach resembles the one presented in the current contribution. Nevertheless they differ in various computational aspects as well as in the specific requirements arising from the design intent.

The remainder of the paper is organized as follows: the modeling of prestressed concrete using equivalent loads is reviewed in Section 2. The problem formulation for simultaneous shape and topology optimization is presented in Section 3, followed by the specific design parametrization and sensitivity analysis in Section 4 and 5. Finally, several design examples are presented and investigated in Section 6 and conclusions are drawn in Section 7.

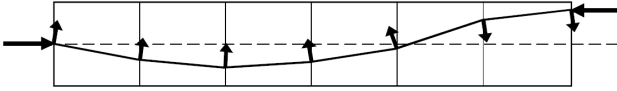
## 2 Modeling prestressed concrete beams

This section is dedicated to a brief review of the modeling approach that was followed in the current study. In essence, a structural beam made of prestressed concrete can be seen as a member made of plain concrete upon which several sets of loads are acting: external “live” loads, such as traffic on a bridge; permanent “dead” loads, such as self-weight; and internal equivalent loads, arising from the action of the prestressing tendon.

Once the prestressing tendon is locked into its position, two concentrated forces act upon the beam at its edges in the locations of the prestressing jacks, admitting compression forces into the beam. The magnitude of these forces is equal to the prestressing force and their direction depends on the geometry of the tendon at its end points. In addition, throughout the span of the beam, the curvature of the tendon creates equivalent forces acting internally on the beam. In typical design applications, the shape of the tendon – encompassing its eccentricity with respect to the beam’s neutral axis and its curvature – is determined such that these

equivalent forces create a deflection that in principle counteracts the deflection due to the load applied on the beam. For example, in a simply supported beam with uniform load, a tendon of parabolic shape will create an upwards deflection that can cancel the downwards deflection due to the external loads.

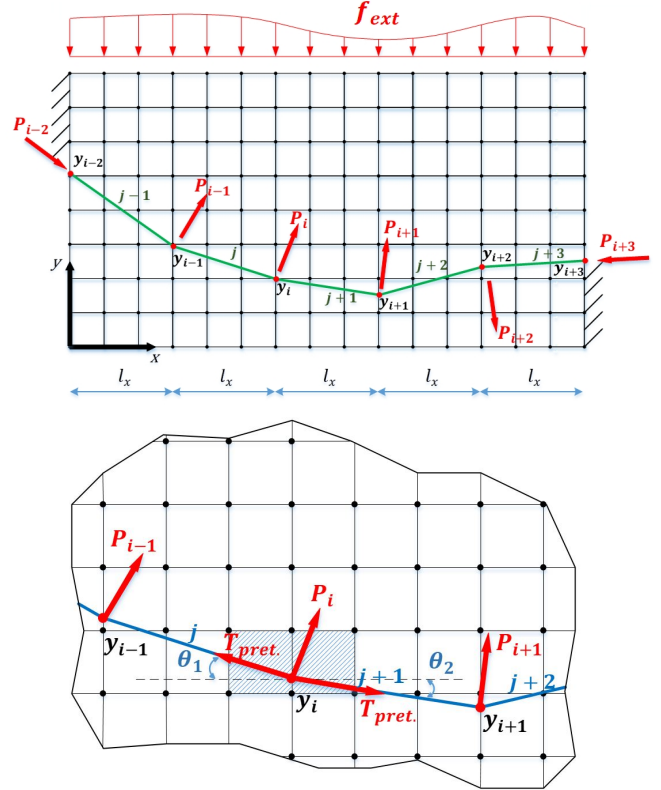
In the current study, the tendon geometry is modeled using a piecewise linear, meaning it is divided into a chain of line segments. The vertical coordinates of the points in the piecewise linear approximation are eventually chosen as shape design variables. Consequently, the internal forces due to curvature are in fact point forces that can be evaluated according to the angle between adjacent linear segments. This choice of parametrization does not imply any loss of generality – the optimization approach can easily accommodate any geometric representation of the tendon. A sketch of the forces acting at end points and at kinks between linear segments is presented in Figure 1.



**Fig. 1** Equivalent forces acting on a beam due to a prestressing tendon, based on a piecewise linear approximation of the tendon with kinks between segments.

For the purpose of continuum topology optimization, it is convenient to represent the concrete domain using a structured grid composed of square finite elements. Then, the horizontal distance between two tendon points is chosen to be constant and the points are located at intersections of the tendon with vertical lines in the structured grid. In the following description, the index  $i$  is assigned to a certain point on the tendon;  $P_i$  is the prestressing force acting on the beam at point  $i$ ;  $y_i$  is the vertical coordinate of the point  $i$ ; the index  $j$  is assigned to a certain segment of the tendon;  $l_x$  is the horizontal projection of the length of each tendon segment; and  $T_{pre}$  is the prestressing force. Force losses along the tendon are neglected in the current study. Nevertheless, immediate losses due to anchorage slip, elastic shortening and friction can be added to the formulation because they depend explicitly on the prestressing force, the concrete deformation and the curvature of the tendon. Furthermore, long-term losses due to creep, shrinkage and relaxation can also be estimated based on tendon forces and concrete deformation. Hence the exact forces along the tendon can be utilized, however it is not evident that there will be any influence on the design. Based on the notation above, the interaction between the tendon and the concrete domain is presented in detail on a portion of the computational grid, see Figure 2. It should be

noted that the coordinates of the tendon points are calculated w.r.t. an origin at the bottom left corner of the domain.



**Fig. 2** The interaction between the tendon and the concrete domain based on the equivalent loads method. Top: A portion of the computational grid; Bottom: A zoom-in on the computation of loads at point  $i$ .

Based on Figure 2, the equations for calculating the prestressing forces acting on the beam are as follows. The length of the  $j$ -th segment is given by

$$l_j = \sqrt{(y_i - y_{i-1})^2 + l_x^2} \quad (1)$$

and the sine and cosine of the angle  $\theta_1$ , corresponding to the  $j$ -th segment, are

$$\sin \theta_1 = \frac{y_{i-1} - y_i}{l_j} \quad (2)$$

$$\cos \theta_1 = \frac{l_x}{l_j}. \quad (3)$$

Similarly, for the subsequent segment we have

$$l_{j+1} = \sqrt{(y_{i+1} - y_i)^2 + l_x^2} \quad (4)$$

$$\sin \theta_2 = \frac{y_{i+1} - y_i}{l_{j+1}} \quad (5)$$

$$\cos \theta_2 = \frac{l_x}{l_{j+1}}. \quad (6)$$

Then, the forces acting upon the beam at point  $i$  are given by

$$P_{i,x} = T_{pret} \times (\cos \theta_2 - \cos \theta_1) \quad (7)$$

$$P_{i,y} = T_{pret} \times (\sin \theta_2 - \sin \theta_1) \quad (8)$$

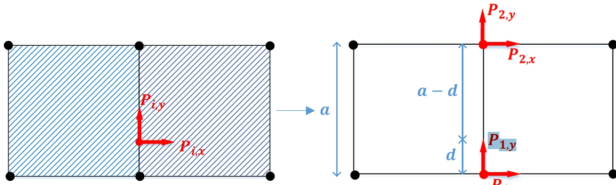
in the  $X$ - and  $Y$ -directions, respectively. Finally, the prestressing forces are transferred to the nodes of the concrete domain using the shape functions of the concrete elements. In the present study a bi-linear approximation of the displacements is used, that reduces to a linear interpolation of nodal values along the elements' edges. Therefore, the prestressing forces applied in a certain point along an element edge can be transferred to the nodes according to the relative distances from the nodes, see also Figure 3:

$$P_{1,x} = P_{i,x} \frac{a-d}{a} \quad (9)$$

$$P_{1,y} = P_{i,y} \frac{a-d}{a} \quad (10)$$

$$P_{2,x} = P_{i,x} \frac{d}{a} \quad (11)$$

$$P_{2,y} = P_{i,y} \frac{d}{a} \quad (12)$$



**Fig. 3** Transferring the loads due to prestressing at point  $i$  to the nearest nodes according to the relative distance.

### 3 Problem formulation

The problem considered in this paper includes simultaneous optimization of both concrete distribution and prestressing tendon geometry. The concrete is modeled as a linear elastic continuum and its response is approximated by means of finite element analysis. While concrete in general exhibits nonlinear response, primarily in tension, it is customary to design prestressed concrete members such that their response is linear-elastic for service loads – namely the concrete remains uncracked. Nevertheless, the methodology presented herein can accommodate inelastic material behavior as implemented in several studies concerning reinforced concrete optimization (Kato et al 2009; Kato and Ramm 2010; Bogomolny and Amir 2012; Amir and Sigmund 2013; Amir 2013). As reviewed in the previous section, the prestressing tendon is modeled by a piecewise linear geometry that

essentially transfers point loads to the concrete medium according to the specific tendon geometry. The stiffness of the tendon itself is neglected for the purpose of design optimization.

The main purpose of prestressing the concrete member is to reduce deformations and subsequent tensile cracking due to the loads that are applied. In principle, for a valid design it is expected that the displacements due to external and self-weight loads, designated herein as  $\mathbf{u}_{ext}$  and  $\mathbf{u}_{sw}$ , will be balanced by the displacements due to the equivalent prestressing loads, designated herein as  $\mathbf{u}_{pre}$ . One can use the external force vector  $\mathbf{f}_{ext}^T$  to quantify the deformation due to external loads on the surface of the beam that admits the load – typically its top side – giving the compliance  $\mathbf{f}_{ext}^T \mathbf{u}_{ext}$  which is the most common objective functional in topology optimization. Similarly, the deformation at the same region due to self-weight and prestressing can be quantified by the products  $\mathbf{f}_{ext}^T \mathbf{u}_{sw}$  and  $\mathbf{f}_{ext}^T \mathbf{u}_{pre}$  respectively, where  $\mathbf{f}_{ext}^T$  essentially measures the total deformation. It should be noted that the magnitude of self-weight forces  $\mathbf{f}_{sw}$  can be scaled properly so that  $\mathbf{f}_{ext}^T \mathbf{u}_{sw}$  will in fact measure the correct deformation on the top surface due to self-weight. A reasonable target is then to minimize the sum of all deformations,  $\mathbf{f}_{ext}^T \mathbf{u}_{total} = \mathbf{f}_{ext}^T (\mathbf{u}_{ext} + \mathbf{u}_{sw} + \mathbf{u}_{pre})$ . If the action of prestressing precisely balances the applied loads, this sum will be zero. In case the displacements  $\mathbf{u}_{ext}$  and  $\mathbf{u}_{sw}$  are dominant,  $\mathbf{f}_{ext}^T \mathbf{u}_{total}$  will be positive and its minimization will be meaningful. In case the displacements  $\mathbf{u}_{pre}$  are dominant,  $\mathbf{f}_{ext}^T \mathbf{u}_{total}$  will be negative and its minimization will lead to flexible designs that exhibit large deformation due to prestressing. Consequently, the objective functional to be minimized is chosen as the square of  $\mathbf{f}_{ext}^T \mathbf{u}_{total}$ .

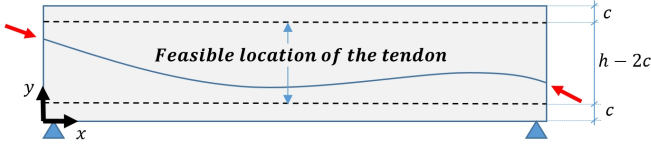
Following the density-based approach to topology optimization (Bendsøe 1989; Bendsøe and Sigmund 2003), the full optimization problem formulation is given by:

$$\begin{aligned} \min_{[\rho, \mathbf{y}]} \quad & \phi = (\mathbf{f}_{ext}^T \mathbf{u}_{total})^2 \\ \text{s.t.:} \quad & g = \frac{\sum_{e=1}^{N_E} \bar{\rho}_e^{dil} v_e}{\sum_{e=1}^{N_E} v_e} - V_{dil}^* \leq 0 \\ & 0 \leq \rho_e \leq 1, \quad e = 1, \dots, N_E \\ & y_i - h + c \leq 0, \quad i = 1, \dots, N_{TP} \\ & -y_i + c \leq 0, \quad i = 1, \dots, N_{TP} \end{aligned} \quad (13)$$

with:  $\mathbf{K}_{ero} \mathbf{u}_{total} = \mathbf{f}_{ext} + \mathbf{f}_{pre} + \mathbf{f}_{sw}$  (14)

where  $\rho$  is the vector of density design variables that determine the concrete's distribution;  $\mathbf{y}$  is the vector of  $Y$ -coordinate design variables that determine the height of each point on the tendon;  $N_E$  and  $N_{TP}$  are the number of continuum finite elements and the number of points on the tendon, respectively;  $\bar{\rho}_e^{dil}$  is a projected dilated density used for imposing the volume constraint on the concrete, and is related to the

mathematical variables  $\rho$  and  $\mathbf{y}$  via filtering and projection operations, see Section 4;  $v_e$  is the volume of the  $e$ -th finite element;  $V_{dil}^*$  is the available volume fraction for the concrete in its dilated configuration;  $h$  is the total height of the beam;  $c$  is the size of the clear concrete cover, defining two (top and bottom) margins in which the tendon cannot be placed – see Figure 4; and  $\mathbf{K}_{ero}$  is the stiffness matrix of the eroded concrete domain, related to the mathematical variables  $\rho$  and  $\mathbf{y}$  via filtering and projection operations, see Section 4.



**Fig. 4** The feasible region for tendon segments such that a clear concrete cover of height  $c$  is maintained at the top and bottom of the beam.

As can be seen in (13), no constraints are imposed on the curvature of the tendons. In principle, it is expected that the tendons' shape should converge towards a piecewise-linear configuration because when the topology converges to a discrete design it essentially interacts with the tendon discontinuously in a series of points. This is visible in the examples in Section 6. Consequently, the tendon has very high curvature in some cases – hence posing manufacturing difficulties. Therefore, curvature constraints can be an important component to be added in future work.

#### 4 Design parametrization

The problem formulation (13) consists of both topological optimization of the concrete and shape optimization of the tendon layout. In order to obtain meaningful results where the tendon is physically embedded into the concrete domain, the two sets of design variables need to be carefully coupled. The sequence of operations that is applied to the design variables in order to obtain the actual physical distribution of concrete, with minimum length scale control, is described in this section.

First, the well-known density filter (Bruns and Tortorelli 2001; Bourdin 2001) is applied to the concrete design variables  $\rho$ , yielding the filtered distribution  $\tilde{\rho}$

$$\tilde{\rho}_i = \frac{\sum_{j \in N_i} w(\mathbf{x}_j) v_j \rho_j}{\sum_{j \in N_i} w(\mathbf{x}_j) v_j} \quad (15)$$

with a linear weighting function

$$w(\mathbf{x}_j) = r_{min} - \|\mathbf{x}_j - \mathbf{x}_i\| \quad (16)$$

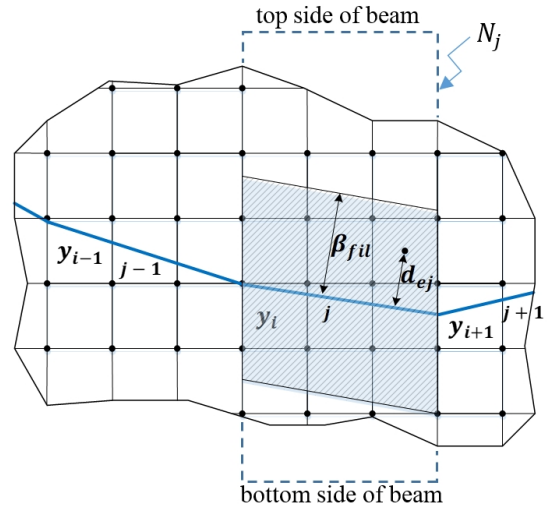
where  $r_{min}$  is the specified filter radius,  $\mathbf{x}_i$  is the position of the centroid of element  $i$  and  $\mathbf{x}_j$  is the position of the centroid

of element  $j$  which is in the neighborhood  $N_i$  of element  $i$  and thus is assigned a positive weight  $w(\mathbf{x}_j)$ .

In the next stage, a special tendon-to-concrete filter operation is performed in order to ensure that the tendon is properly covered by concrete. The idea is related to a previous development of a filter that relates the existence of steel bars to the existence of concrete in their surroundings, in the context of reinforced concrete topology optimization (Amir 2013). In the current approach, the location of each tendon segment defines a region to which concrete is projected. The projection is defined by a Super-Gaussian function,

$$\hat{\rho}_{i \in N_j} = \tilde{\rho}_i + (1 - \tilde{\rho}_i) e^{-\frac{1}{2} \left( \frac{d_{ij}}{\beta_{fil}} \right)^{\mu_{pre}}} \quad (17)$$

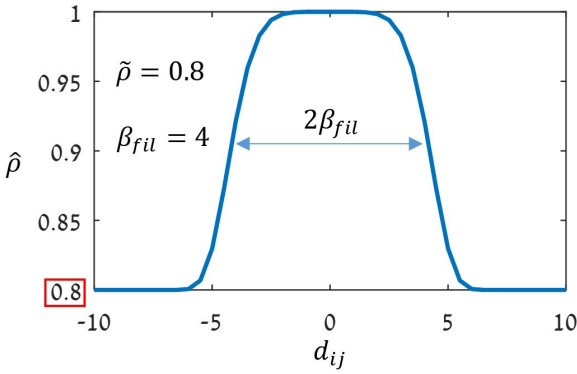
where  $\hat{\rho}_i$  is the density of the  $i$ -th element after the tendon-to-concrete filtering;  $N_j$  is the neighborhood of the  $j$ -th tendon segment;  $d_{ij}$  the shortest distance between the center of the  $i$ -th continuum element and the  $j$ -th tendon segment;  $\beta_{fil}$  is an influence length that represents the width of the tendon-to-concrete filter in the direction perpendicular to the tendon segment; and  $\mu_{pre}$  is the sharpness of the Super-Gaussian function. A graphical description of the tendon-to-concrete filter is presented in Figure 5 and an example of the function (17) is presented in Figure 6. Using the function (17), the densities of elements in the vicinity of a tendon segment are pushed to 1.0 whereas elements that are outside the influenced region remain unchanged.



**Fig. 5** The tendon-to-concrete filter that ensures the tendon will be properly covered by concrete. The neighborhood  $N_j$  is defined as the rectangular domain encompassing the  $j$ -th segment of the tendon through the complete beam height.

In the final stage, we apply smooth Heaviside projection functions that assists in obtaining a distinct 0-1 (or void-solid) layout (Guest et al 2004; Xu et al 2010). In partic-





**Fig. 6** An example of the tendon-to-concrete filter function, for an input density  $\tilde{\rho} = 0.8$  and influence distance of  $\beta_{fil} = 4$ . In the vicinity of the tendon segment ( $-4 \leq d_{ij} \leq 4$ ), the density of concrete is gradually increased to 1.0.

ular, we apply the robust topology optimization approach where eroded and dilated layouts are added to a worst-case formulation (Wang et al 2011). This guarantees control over minimum length scale and for problems involving only stiffness and volume one can simply use the eroded design for quantifying the worst case for stiffness whereas the dilated design quantifies the worst case for volume (Lazarov et al 2016). Therefore, the densities after tendon-to-concrete filtering are further projected to obtain the eroded and dilated densities respectively,

$$\bar{\rho}_i^{ero} = \frac{\tanh(\beta_{HS}\eta_{ero}) + \tanh(\beta_{HS}(\hat{\rho}_i - \eta_{ero}))}{\tanh(\beta_{HS}\eta_{ero}) + \tanh(\beta_{HS}(1 - \eta_{ero}))} \quad (18)$$

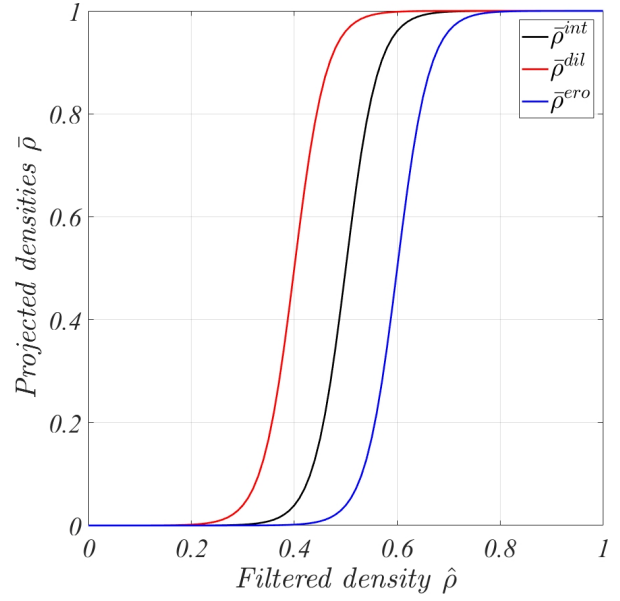
$$\bar{\rho}_i^{dil} = \frac{\tanh(\beta_{HS}\eta_{dil}) + \tanh(\beta_{HS}(\hat{\rho}_i - \eta_{dil}))}{\tanh(\beta_{HS}\eta_{dil}) + \tanh(\beta_{HS}(1 - \eta_{dil}))} \quad (19)$$

where  $\beta_{HS}$  governs the curvature of the smooth projection;  $\eta_{ero}$  is the projection threshold for the eroded layout (e.g.  $\eta_{ero} = 0.6$ ); and  $\eta_{dil}$  is the projection threshold for the dilated layout (e.g.  $\eta_{dil} = 0.4$ ). We note that the response of the actual (or intermediate, with  $\bar{\rho}^{int}$ ) design intended for manufacturing need not be evaluated during the optimization. It is computed only for adapting the volume constraint and for applying self-weight, according to the same projection function but with  $\eta = 0.5$ . A graphical demonstration of the erosion and dilation projection functions is presented in Figure 7.

For evaluating the structural response by Eq. (14), Young's modulus of each concrete element in the eroded layout is determined by the Modified SIMP interpolation rule (Sigmund and Torquato 1997),

$$E(\bar{\rho}^{ero}) = E_{min} + (E_{max} - E_{min})(\bar{\rho}^{ero})^{p_E} \quad (20)$$

where  $E_{min}$  is a relatively small positive number in order to avoid singularity of the stiffness matrix;  $E_{max}$  is the actual value of Young's modulus for concrete; and  $p_E$  is a penalization factor that drives the design towards a 0-1 distribution.



**Fig. 7** A graphical illustration of the smooth projection functions, used in order to achieve minimum length scale and crisp void-solid layouts.

## 5 Sensitivity analysis

In this section we provide some details regarding the sensitivity analysis procedure. As inferred from the design parametrization, both the objective and the volume constraint involve a coupling between topological density variables that govern the distribution of concrete and shape variables that govern the position of the tendon. This is due to the tendon-to-concrete filtering that generates a dependence of the concrete distribution on the tendon position. For general derivations in this section, design variables are grouped in the vector  $\mathbf{x}$ . Towards the end of the section, specific derivatives with respect to the variables  $[\rho, \mathbf{y}]$  are presented.

For differentiating the objective functional, we follow the adjoint method. First, an augmented objective functional is defined as

$$\hat{\phi}(\mathbf{x}) = (\mathbf{f}_{ext}^T \mathbf{u}_{total})^2 + \lambda^T (\mathbf{K}_{ero} \mathbf{u}_{total} - \mathbf{f}_{ext} - \mathbf{f}_{pre} - \mathbf{f}_{sw}) \quad (21)$$

where  $\lambda$  is the adjoint vector. The partial derivative with respect to a certain variable  $x_i$  is given by

$$\begin{aligned} \frac{\partial \hat{\phi}}{\partial x_i} = & 2\mathbf{f}_{ext}^T \mathbf{u}_{total} \mathbf{f}_{ext}^T \frac{\partial \mathbf{u}_{total}}{\partial x_i} + \lambda^T \left( \frac{\partial \mathbf{K}_{ero}}{\partial x_i} \mathbf{u}_{total} \right. \\ & \left. + \mathbf{K}_{ero} \frac{\partial \mathbf{u}_{total}}{\partial x_i} - \frac{\partial \mathbf{f}_{pre}}{\partial x_i} - \frac{\partial \mathbf{f}_{sw}}{\partial x_i} \right). \end{aligned} \quad (22)$$

In order to eliminate the parts that involve implicit derivatives of the displacements, namely  $\frac{\partial \mathbf{u}_{total}}{\partial x_i}$ , the following adjoint equation is to be solved,

$$\mathbf{K}_{ero}^T \lambda = -2\mathbf{f}_{ext} \mathbf{u}_{total}^T \mathbf{f}_{ext}. \quad (23)$$

Once the adjoint vector is computed, it can be substituted back to Eq. (22), giving an expression that contains only explicit derivatives,

$$\frac{\partial \hat{\phi}}{\partial x_i} = \lambda^T \frac{\partial \mathbf{K}_{ero}}{\partial x_i} \mathbf{u}_{total} - \lambda^T \frac{\partial \mathbf{f}_{pre}}{\partial x_i} - \lambda^T \frac{\partial \mathbf{f}_{sw}}{\partial x_i}. \quad (24)$$

The explicit derivatives appearing in Eq. (24) are computed by chain rules. For a certain topological variable  $\rho_i$ , the derivative of the stiffness is given by

$$\frac{\partial \mathbf{K}_{ero}}{\partial \rho_i} = \sum_{e \in N_i} \frac{\partial \mathbf{K}_{ero}}{\partial \bar{\rho}_e^{ero}} \frac{\partial \bar{\rho}_e^{ero}}{\partial \hat{\rho}_e} \frac{\partial \hat{\rho}_e}{\partial \tilde{\rho}_e} \frac{\partial \tilde{\rho}_e}{\partial \rho_i} \quad (25)$$

where the components can be evaluated explicitly as follows:

- $\frac{\partial \mathbf{K}_{ero}}{\partial \bar{\rho}_e^{ero}}$  is related to the interpolation rule (20) for the stiffness;
- $\frac{\partial \bar{\rho}_e^{ero}}{\partial \hat{\rho}_e}$  is related to the smooth Heaviside projection (18);
- $\frac{\partial \hat{\rho}_e}{\partial \tilde{\rho}_e}$  is related to the tendon-to-concrete filter (17);
- $\frac{\partial \tilde{\rho}_e}{\partial \rho_i}$  is the derivative of the density filter (15);
- $\sum_{e \in N_i}$  is the collection of derivatives within the neighborhood of the  $i$ -th element in the density filter function.

For a certain shape variable  $y_i$ , the derivative of the stiffness is given by another chain rule,

$$\frac{\partial \mathbf{K}_{ero}}{\partial y_i} = \sum_{e \in N_i} \frac{\partial \mathbf{K}_{ero}}{\partial \bar{\rho}_e^{ero}} \frac{\partial \bar{\rho}_e^{ero}}{\partial \hat{\rho}_e} \frac{\partial \hat{\rho}_e}{\partial y_i} \quad (26)$$

where the first two components are as defined above. The third component is the collection of derivatives of Eq. (17), related to elements  $e$  that are influenced by the  $i$ -th tendon coordinate, i.e. in the neighborhoods of its adjacent tendon segment or segments. Essentially, this derivative is defined by the distance  $d_{ej}$  between the element  $e$  and the segment  $j$ , see also Figure 5.

As for the derivatives of the force vectors, the prestressing forces  $\frac{\partial \mathbf{f}_{pre}}{\partial x_i}$  have zero derivative w.r.t. topological variables whereas w.r.t. shape variables it is a straightforward derivative based on the geometric relations in Section 2. In case self-weight loads are applied, their force vector has derivatives w.r.t. both topological as well as shape variables. These derivatives will take a form similar to Eqs. (25) and (26), just that the first component will be related to the dependency of the force on the physical material distribution. For example, if the intermediate layout is used for computing gravity loads, then we have

$$\frac{\partial \mathbf{f}_{sw}}{\partial \rho_i} = \sum_{e \in N_i} \frac{\partial \mathbf{f}_{sw}}{\partial \bar{\rho}_e^{int}} \frac{\partial \bar{\rho}_e^{int}}{\partial \hat{\rho}_e} \frac{\partial \hat{\rho}_e}{\partial \tilde{\rho}_e} \frac{\partial \tilde{\rho}_e}{\partial \rho_i} \quad (27)$$

$$\frac{\partial \mathbf{f}_{sw}}{\partial y_i} = \sum_{e \in N_i} \frac{\partial \mathbf{f}_{sw}}{\partial \bar{\rho}_e^{int}} \frac{\partial \bar{\rho}_e^{int}}{\partial \hat{\rho}_e} \frac{\partial \hat{\rho}_e}{\partial y_i} \quad (28)$$

where the first component can be evaluated straightforwardly on an element-by-element basis.

As for the volume constraint, following (13) it can be seen that the volume depends directly on the dilated densities. Accordingly, its derivatives will take the form

$$\frac{\partial g}{\partial \rho_i} = \sum_{e \in N_i} \frac{\partial g}{\partial \bar{\rho}_e^{dil}} \frac{\partial \bar{\rho}_e^{dil}}{\partial \hat{\rho}_e} \frac{\partial \hat{\rho}_e}{\partial \tilde{\rho}_e} \frac{\partial \tilde{\rho}_e}{\partial \rho_i} \quad (29)$$

$$\frac{\partial g}{\partial y_i} = \sum_{e \in N_i} \frac{\partial g}{\partial \bar{\rho}_e^{dil}} \frac{\partial \bar{\rho}_e^{dil}}{\partial \hat{\rho}_e} \frac{\partial \hat{\rho}_e}{\partial y_i} \quad (30)$$

where the first terms are straightforward and the following terms arise from Eqs. (19), (17) and (15).

## 6 Examples

In this section we present several demonstrative examples that expose the capability of the suggested formulation to achieve simultaneous optimization of the tendon shape and the concrete topology. For optimization in the nested approach, we use the Method of Moving Asymptotes (MMA, Svanberg (1987)). Because the evolution of shape and topology are strongly coupled, we apply relatively conservative external move limits of 0.2 and 0.05 on shape and topology variables, respectively.

Throughout all examples we use a continuation scheme on the parameters that control the sharpness of the SIMP penalty, the smooth Heaviside projections and the tendon-to-concrete filtering. The penalty  $p_E$  in the SIMP interpolation function begins at 1.0 and is increased by 0.5 every 25 design cycles, up to a maximum value of 3.0. The parameter  $\beta_{HS}$  begins at 1.0 and is increased by 1.0 every 25 design cycles, up to a maximum value of 8.0. The parameter  $\mu_{pre}$  in Eq. (17) begins at 1.0 and is increased by 1.0 every 25 design cycles, up to a maximum value of 4.0. In all examples, the number of design iterations is fixed to 200 – allowing for the continuation scheme to facilitate stable convergence. The parameter  $\beta_{fil}$  is constant and is equal to  $r_{min}$ , so that length scale in the vicinity of the tendon is consistent with the overall design. The allowable volume of the dilated design  $V_{dil}^*$  is continuously adapted such that the volume of the intermediate design will eventually meet its allowable volume fraction. The Heaviside projection functions are computed with  $\eta_{dil} = 0.4$  and  $\eta_{ero} = 0.6$ .

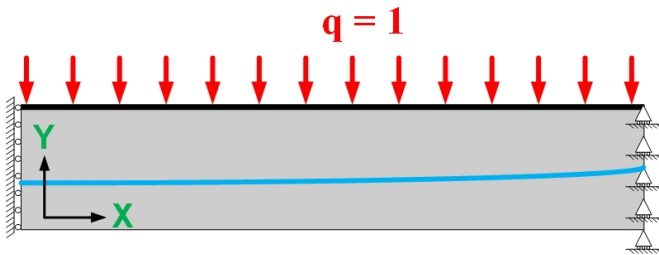
In all examples, the material properties are set to  $E_{max} = 30,000$ ,  $E_{min} = 0.3$  and  $\nu = 0.2$ . An initial assessment of a suitable prestressing force is based on formulas for standard beams with uniform cross section. For example, for a simply-supported beam with rectangular cross-section, the requirement that in mid-span there will be zero tensile stresses at the bottom chord leads to

$$T_{STD} = \frac{M_{total}}{e + \frac{h}{6}} \quad (31)$$

where  $T_{STD}$  stands for the prestressing force of a standard beam;  $M_{total}$  is the total bending moment due to external forces and self-weight;  $e$  is the eccentricity of the tendon w.r.t. the cross-section's neutral axis; and  $h$  is the total height of the section. Clearly, this formula does not account for topological changes but can provide an estimate for the required prestressing force – because it will cancel the bending moments in a non-optimized uniform beam. As a default in all examples, the shape of the prestressing tendon is parametrized by its  $Y$ -coordinate every 10 elements in the  $X$ -direction. The  $Y$ -coordinates of the tendon cannot penetrate into a clear cover region of 2 elements in the top and bottom of the design domain.

### 6.1 Example 1: Simply-supported beam under uniform load

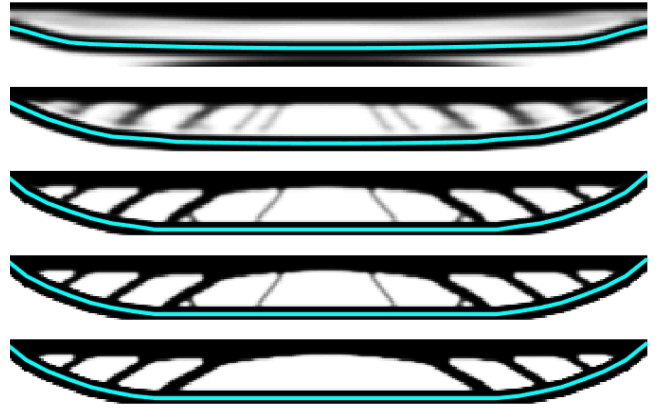
In the first example we demonstrate the design of a single-span simply supported beam subjected to a uniform load. The setup of the problem is presented in Figure 8. Note that sliding supports are available through the whole height of the beam, so to enable the optimization to choose the best location of the support that will coincide with the tendon's anchor. Providing a single support at the bottom of the beam will require a somewhat artificial vertical connection between the support and the anchoring point. The beam has a length-to-height ratio of 10:1 and it is modeled using a structured grid of  $300 \times 30$  square finite elements with side length of unity. In practice, only half of the domain is optimized due to symmetry. The magnitude of the uniform external load is  $q = 1.0$ , acting in the  $-Y$  direction. For bearing the uniform load, the top 4 layers of elements are fixed to be solid material. The filter radius  $r_{min}$  is set to 3.0 and the allowable volume fraction is 50%.



**Fig. 8** Setup for the optimization of a single-span simply supported beam subjected to a uniform load. Only the right symmetric half is presented. The black region is fixed solid, the gray region is design concrete and the blue line is the tendon configuration.

The optimization is executed with five different values of the prestressing force, spanning the range from  $T_{pre} = 0.6 \times T_{STD}$  to  $T_{pre} = 1.4 \times T_{STD}$ . Results from the optimization are summarized in Table 1 and snapshots from selected

design cycles are displayed in Figure 9. The effect of the prestressing force is evident: for lower values, the minimization is driven mainly by the compliance of the external forces while the prestressing force is not large enough in order to completely balance the deformation. In contrast, for higher prestressing forces the attained objective value approaches zero and the two deformations are practically balanced. It can be seen that the optimization no longer seeks “the stiffest design” – the results with  $T_{pre} = 1.2 \times T_{STD}$  and  $T_{pre} = 1.4 \times T_{STD}$  are more compliant w.r.t. the external loads. Furthermore, non-uniqueness of the solution arises because there can exist multiple layouts that exhibit a balance of deformations. As the topological layout is not driven to be the stiffest anymore, also convergence to void-solid is not guaranteed because the underlying principle of SIMP and the projection functions is not applicable. In conclusion, results indicate that the estimate  $T_{pre} = 1.0 \times T_{STD}$  works quite well for this problem and leads to a stiff layout whose deformation due to prestressing nearly cancels out the deformation due to the uniform load. Clearly, one can consider the prestressing force as an additional design variable however this aspect is out of the scope of the current contribution.








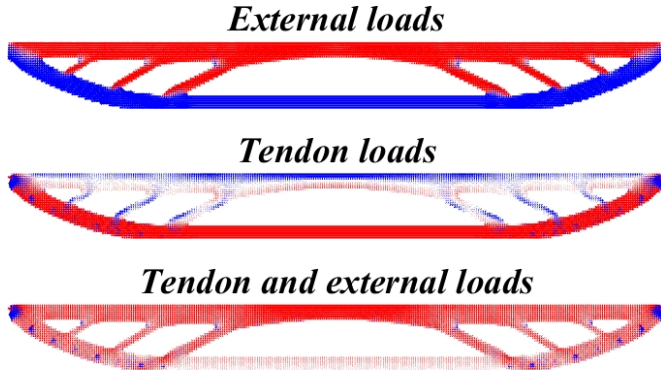
**Fig. 9** Snapshots of the optimization process with  $T_{pre} = 0.8 \times T_{STD}$  after 25, 50, 75, 100 and 125 design cycles.

Principal stress plots for the optimized design with  $T_{pre} = 0.8 \times T_{STD}$  are presented in Figure 10. When only the uniform load is applied, high tensile stresses appear in the bottom chord of the beam. The prestressing itself introduces high compressive stresses at the bottom chord, whereas the upper part of the layout is acting in shear and bending – resulting from the concentrated forces that are transferred from the tendon to the diagonal struts. Summing up both actions, the compressive stresses at the bottom chord are small and the whole structure is essentially in a compressive state, except for a few local stress concentrations at the connections between the tendon and the plain concrete. Therefore the desirable effect of prestressing is achieved.



**Table 1** Optimization of a simply-supported beam with uniform load and various values of the prestressing force.

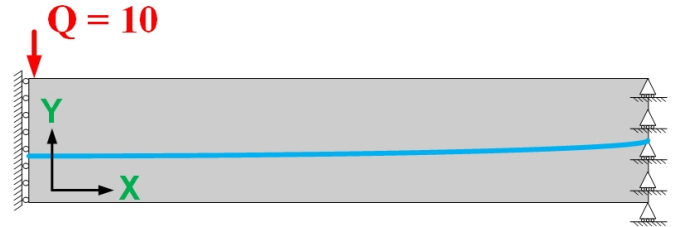
Case			optimized layout
$T_{pre} = 0.6 \times T_{STD}$	$\phi$	8.1490e+03	
	$\mathbf{f}_{ext}^T \mathbf{u}_{ext}$	204.6562	
	$\mathbf{f}_{ext}^T \mathbf{u}_{pre}$	-114.3846	
$T_{pre} = 0.8 \times T_{STD}$	$\phi$	2.9178e+03	
	$\mathbf{f}_{ext}^T \mathbf{u}_{ext}$	211.6173	
	$\mathbf{f}_{ext}^T \mathbf{u}_{pre}$	-157.6005	
$T_{pre} = 1.0 \times T_{STD}$	$\phi$	2.0800e+02	
	$\mathbf{f}_{ext}^T \mathbf{u}_{ext}$	213.1219	
	$\mathbf{f}_{ext}^T \mathbf{u}_{pre}$	-198.6995	
$T_{pre} = 1.2 \times T_{STD}$	$\phi$	4.9464e-05	
	$\mathbf{f}_{ext}^T \mathbf{u}_{ext}$	222.6423	
	$\mathbf{f}_{ext}^T \mathbf{u}_{pre}$	-222.6353	
$T_{pre} = 1.4 \times T_{STD}$	$\phi$	1.0854e-04	
	$\mathbf{f}_{ext}^T \mathbf{u}_{ext}$	251.9399	
	$\mathbf{f}_{ext}^T \mathbf{u}_{pre}$	-251.9295	

**Fig. 10** Principal stress plots of the simply-supported beam optimized with  $T_{pre} = 0.8 \times T_{STD}$ . Red represents compression, blue represents tension. Without prestressing, high tensile stresses appear in the bottom chord. With prestressing, the whole beam is in a compressive state, except for local bi-axial stress concentrations.

## 6.2 Example 2: Simply-supported beam under concentrated load

The second example shows the optimized design of a single-span simply supported beam subjected to a concentrated load. The setup of the problem is presented in Figure 11. All parameters are the same as in the previous case, except for the external loading that is replaced by a point load with a magnitude of  $Q = 10$ , acting in the  $-Y$  direction. Fixed solids in the top layers are therefore not necessary. The optimization was performed with various values of the prestressing force between  $0.5 \times T_{STD}$  and  $1.5 \times T_{STD}$ .

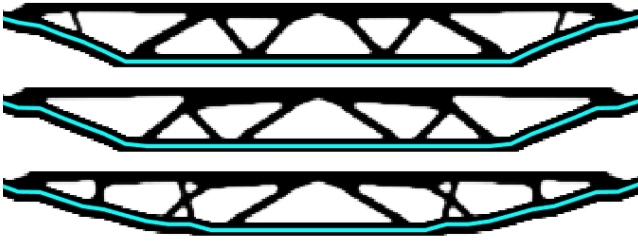
Three of the optimized designs obtained for the beam are displayed in Figure 12. It is interesting to see how the designs that have a lower available prestressing force, create an internal MBB-like structure which is known to be very stiff for concentrated forces. The internal MBB-like

**Fig. 11** Setup for the optimization of a single-span simply supported beam subjected to a concentrated load. Only the right symmetric half is presented. The gray region is designable concrete and the blue line is the tendon configuration.

layout is then connected to the supports by diagonal tendons. Similar to the previous results, the layouts generated with smaller prestressing forces are stiffer w.r.t. the point load, but their overall objective is higher. Another interesting aspect is the adaptation of the topological layout to high prestressing forces. The design generated for  $T_{pre} = 1.5 \times T_{STD}$  contains X-like braces that connect the prestressing tendon to the top chord. As can be seen in the stress plots in Figure 10, the response in these regions is dominated by shear. Consequently, when the shear stresses are high due to high prestressing forces, the X-bracing is chosen because of its superior resistance to shear.

## 6.3 Example 3: Two-span continuous beam under uniform load

In this example we show the design of a statically indeterminate structure, namely a two-span beam subjected to a uniform load. The setup of the problem is presented in Figure 13. The beam is modeled using a structured grid of  $800 \times 40$  square finite elements with side length of unity. In practice,



**Fig. 12** Optimized designs with a point load, obtained with various values of  $T_{pre}$ . From top:  $0.5 \times T_{STD}$ ,  $\phi = 4.1508$ ;  $1.0 \times T_{STD}$ ,  $\phi = 1.9516$ ;  $1.5 \times T_{STD}$ ,  $\phi = 0.9436$ .

only half of the domain is optimized due to symmetry. The magnitude of the uniform external load is  $q = 1.0$ , acting in the  $-Y$  direction. For admitting the uniform load, the top 4 layers of elements are fixed to be solid material. The filter radius  $r_{min}$  is set to 4.0 so that the same physical length scale is imposed as in the previous examples, and the allowable volume fraction is 50%. The prestressing force is determined based on the assumption (31), multiplied by 0.8. This reduction is due to the fact that the maximum bending moments that appears above the central support are in practice reduced because of the local influence of the support width.

The evolution of the optimized design obtained for the two-span beam is displayed in Figure 14. The compliance is  $\mathbf{f}_{ext}^T \mathbf{u}_{ext} = 355.2403$ , the product of external forces over prestressing displacements is  $\mathbf{f}_{ext}^T \mathbf{u}_{pre} = -354.9260$ , giving a final objective value of  $\phi = 0.0988$ . As the results indicate, the deformation due to external loads is nearly canceled out by the deformation due to prestressing. Furthermore, it can be seen that the shape of the tendon and the continuum topology adapt to each other symbiotically, both for tensile stresses within the beam spans (causing tension in the bottom chord) as well as for tensile stresses above the central support (causing tension in the top chord).

In the following we examine a similar beam as in the previous case, with the addition of gravity loads. The purpose is to see how the topological layout and the tendon shape adapt according to a design-dependent loading, in particular when its magnitude is significantly larger than that of the fixed external loads. The majority of parameters remain the same as in the previous case. One exception is the beam domain which is modeled using a structured grid of  $480 \times 30$  square finite elements with side length of unity. The filter radius  $r_{min}$  is reduced accordingly to 3.0. Again, symmetry is applied so only half of the domain is simulated and optimized.

The optimized beam with only a uniform load of  $q = 1.0$  serves as a reference solution and is presented in the top of Figure 15. As can be observed, it strongly resembles the solution above that had slightly longer span and finer mesh resolution. Next, self-weight is applied in addition to the uniform load. In order to create a design scenario in which

gravity is the dominant load in comparison to live loads, the magnitude of the self-weight load is scaled so that each node will receive a contribution of  $4.0 \times \bar{\rho}^{int}$  from each adjacent element. This leads to a total gravity load which is roughly two orders of magnitude larger than the uniform load. Accordingly, the prestressing force is computed as before based on the bending moments due to the uniform load, and then multiplied by 50. The optimized design for these parameters is presented in the bottom of Figure 15. The objective functional reached a value of  $\phi = 1.545e-03$ , indicating that the prestressing forces nearly cancel the deformation due to external and self-weight loads. More specifically, the objective is composed of  $\mathbf{f}_{ext}^T \mathbf{u}_{ext} = 77.0197$ ,  $\mathbf{f}_{ext}^T \mathbf{u}_{sw} = 3.4122e+03$  and  $\mathbf{f}_{ext}^T \mathbf{u}_{pre} = -3.4892e+03$ . Therefore, the approach suggested herein succeeds in finding optimized designs also for cases that are dominated by gravity while the external load is almost negligible. Comparing the optimized layout to the one without self-weight, it can be observed that more material is positioned near the central support so that deformation due to self-weight is reduced.

## 7 Conclusions

A new methodology and computational procedure for optimizing prestressed concrete structures was presented. The problem formulation combines both shape optimization of the prestressing tendon and topology optimization of the concrete layout. The tendon is treated as a collection of equivalent loads that act internally on the beam as a result of the tendon's curvature. A special filtering technique is introduced for constraining the tendon to be properly covered by concrete, thus adding a coupling between shape and topological variables.

The applicability of the proposed method is demonstrated on several test cases. The results presented in Section 6 indicate that the optimization successfully reaches topological layouts for which the deformation due to the applied loads is balanced by the deformation due to prestressing. Furthermore, principal stress plots show that the desired effect of a fully compressed structure is achieved. The influence of the magnitude of the prestressing forces is also demonstrated and investigated. For small prestressing forces, the design is primarily stiffened against the external loads while the prestressing only reduces the overall deformation. Once high prestressing forces are applied, the design is more compliant with respect to the external loads but the prestressing can lead to practically zero total deformation.

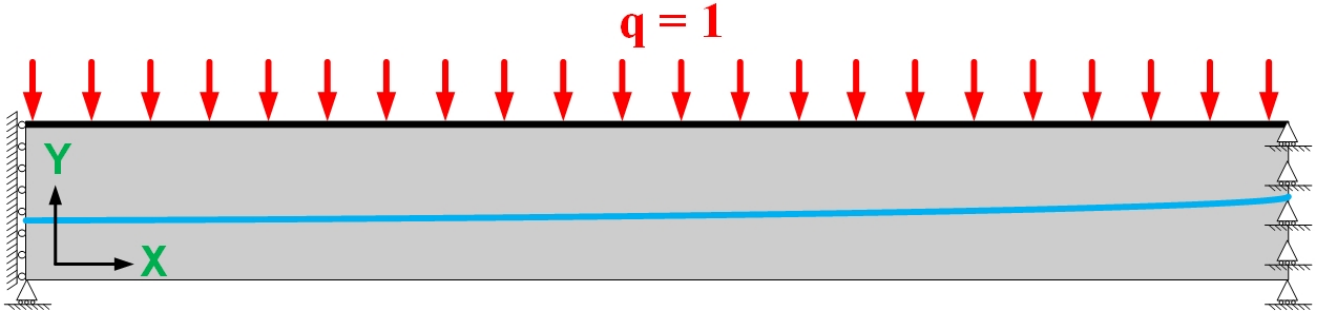
The framework presented herein is rather general and can open many possibilities for future extensions. These include the treatment of the prestressing force as a design variable, and the investigation of other objective functionals for quantifying the design intent of prestressed concrete members. In principle, the formulation can be applied to three-

dimensional problems. Nevertheless, the simultaneous optimization of multiple tendons can raise some difficulties regarding intersections, overlapping and proximity of tendons – hence this is by no means a straightforward extension. More rigorous geometric representations may be helpful in managing the parametrization and the various constraints. On a wider scope, the coupled shape-topology framework could be applied to other classes of problems in which it is beneficial to embed discrete segments within the surrounding continuum.

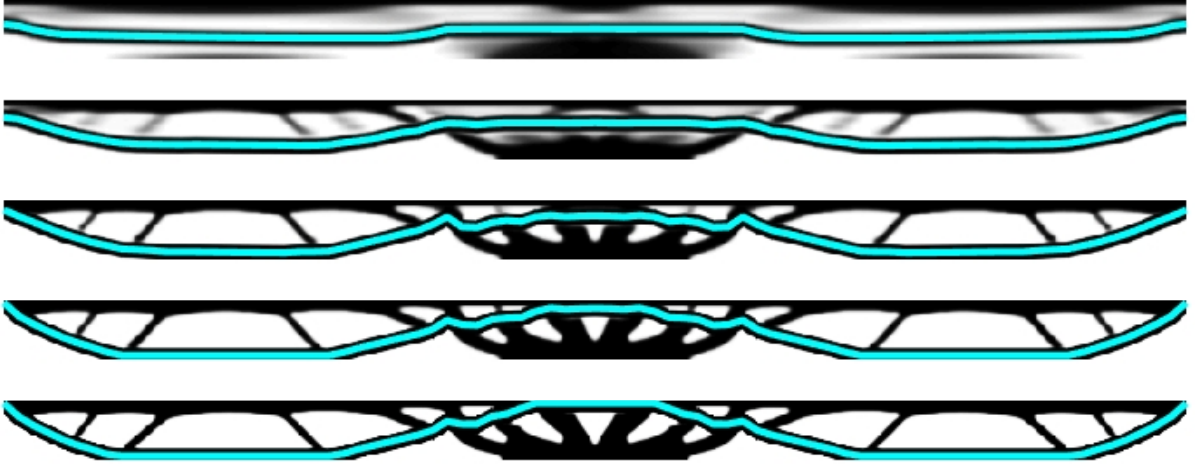
## References

- Amir O (2013) A topology optimization procedure for reinforced concrete structures. *Computers & Structures* 114–115:46–58, DOI <http://dx.doi.org/10.1016/j.compstruc.2012.10.011>, URL <http://www.sciencedirect.com/science/article/pii/S0045794912002337>
- Amir O, Sigmund O (2013) Reinforcement layout design for concrete structures based on continuum damage and truss topology optimization. *Structural and Multidisciplinary Optimization* 47(2):157–174, DOI 10.1007/s00158-012-0817-1, URL <http://dx.doi.org/10.1007/s00158-012-0817-1>
- Bendsøe MP (1989) Optimal shape design as a material distribution problem. *Structural optimization* 1(4):193–202
- Bendsøe MP, Kikuchi N (1988) Generating optimal topologies in structural design using a homogenization method. *Computer methods in applied mechanics and engineering* 71(2):197–224
- Bendsøe MP, Sigmund O (2003) *Topology Optimization - Theory, Methods and Applications*. Springer, Berlin
- Bogomolny M, Amir O (2012) Conceptual design of reinforced concrete structures using topology optimization with elastoplastic material modeling. *International Journal for Numerical Methods in Engineering* 90(13):1578–1597, DOI 10.1002/nme.4253, URL <http://dx.doi.org/10.1002/nme.4253>
- Bourdin B (2001) Filters in topology optimization. *International Journal for Numerical Methods in Engineering* 50:2143–2158
- Bruggi M (2009) Generating strut-and-tie patterns for reinforced concrete structures using topology optimization. *Computers and Structures* 87(23–24):1483–1495
- Bruggi M (2016) A numerical method to generate optimal load paths in plain and reinforced concrete structures. *Computers & Structures* 170:26–36
- Bruns TE, Tortorelli DA (2001) Topology optimization of non-linear elastic structures and compliant mechanisms. *Computer Methods in Applied Mechanics and Engineering* 190:3443–3459
- Cohn M, Lounis Z (1993) Optimum limit design of continuous prestressed concrete beams. *Journal of structural engineering* 119(12):3551–3570
- Deaton J, Grandhi R (2014) A survey of structural and multidisciplinary continuum topology optimization: post 2000. *Structural and Multidisciplinary Optimization* 49(1):1–38, DOI 10.1007/s00158-013-0956-z, URL <http://dx.doi.org/10.1007/s00158-013-0956-z>
- Du J, Olhoff N (2004) Topological optimization of continuum structures with design-dependent surface loading—part i: new computational approach for 2d problems. *Structural and Multidisciplinary Optimization* 27(3):151–165
- Eurviriyankul S, Askes H (2010) The equilibration of configurational forces in the tendon layout optimisation of pre-stressed concrete beams. *Computers & structures* 88(23):1412–1418
- Eurviriyankul S, Askes H (2011) Tendon layout optimisation through configurational forces equilibration in plane stress analysis of prestressed concrete structures. *Computers & Structures* 89(17):1673–1680
- Flower DJ, Sanjayan JG (2007) Green house gas emissions due to concrete manufacture. *The international Journal of life cycle assessment* 12(5):282
- Gaynor AT, Guest JK, Moen CD (2012) Reinforced concrete force visualization and design using bilinear truss-continuum topology optimization. *Journal of Structural Engineering* 139(4):607–618
- Guest JK, Prévost JH, Belytschko T (2004) Achieving minimum length scale in topology optimization using nodal design variables and projection functions. *International Journal for Numerical Methods in Engineering* 61:238–254
- Kato J, Ramm E (2010) Optimization of fiber geometry for fiber reinforced composites considering damage. *Finite Elements in Analysis and Design* 46(5):401–415
- Kato J, Lipka A, Ramm E (2009) Multiphase material optimization for fiber reinforced composites with strain softening. *Structural and Multidisciplinary Optimization* 39(1):63–81
- Kirsch U (1972) Optimum design of prestressed beams. *Computers & Structures* 2(4):573–583
- Kirsch U (1973) Optimized prestressing by linear programming. *International Journal for Numerical Methods in Engineering* 7(2):125–136
- Lazarov BS, Wang F, Sigmund O (2016) Length scale and manufacturability in density-based topology optimization. *Archive of Applied Mechanics* 86(1–2):189–218
- Lee E, Martins JR (2012) Structural topology optimization with design-dependent pressure loads. *Computer Methods in Applied Mechanics and Engineering* 233:40–48
- Liang Q, Xie Y, Steven G (2000) Topology optimization of strut-and-tie models in reinforced concrete structures using an evolutionary procedure. *ACI Structural journal* 97(2):322–330
- Liang QQ, Xie YM, Steven GP (2001) Generating optimal strut-and-tie models in prestressed concrete beams by performance-based optimization. *ACI Structural Journal* 98(2):226–232
- Liu S, Qiao H (2011) Topology optimization of continuum structures with different tensile and compressive properties in bridge layout design. *Structural and Multidisciplinary Optimization* 43:369–380, DOI 10.1007/s00158-010-0567-x
- Luo Y, Kang Z (2012) Layout design of reinforced concrete structures using two-material topology optimization with druckerprager yield constraints. *Structural and Multidisciplinary Optimization online*, DOI 10.1007/s00158-012-0809-1, published online
- Luo Y, Wang MY, Zhou M, Deng Z (2015) Topology optimization of reinforced concrete structures considering control of shrinkage and strength failure. *Computers & Structures* 157:31–41
- Mahasanen N, Smith S, Humphreys K (2003) The cement industry and global climate change: Current and potential future cement industry CO<sub>2</sub> emissions. In: Gale J, Kaya Y (eds) *Greenhouse Gas Control Technologies - 6th International Conference*, Pergamon, Oxford, pp 995–1000, DOI 10.1016/B978-008044276-1/50157-4, URL <http://www.sciencedirect.com/science/article/pii/B9780080442761501574>
- Moorman RB (1952) Equivalent load method for analyzing prestressed concrete structures. In: *Journal Proceedings*, vol 48, pp 405–416
- Sigmund O, Bendsøe MP (2004) Topology optimization: from air-planes to nano-optics. In: Stubbkær K, Kortenbach T (eds) *Bridging from Technology to Society*, Technical University of Denmark, Lyngby, Denmark
- Sigmund O, Maute K (2013) Topology optimization approaches. *Structural and Multidisciplinary Optimization* 48(6):1031–1055
- Sigmund O, Torquato S (1997) Design of materials with extreme thermal expansion using a three-phase topology optimization method. *Journal of the Mechanics and Physics of Solids* 45(6):1037–1067
- Stocker TF, Qin D, Plattner GK, Tignor M, Allen SK, Boschung J, Nauels A, Xia Y, Bex B, Midgley B (2013) IPCC, 2013: Climate

- Change 2013: The physical science basis. Contribution of working group I to the fifth assessment report of the intergovernmental panel on climate change. Cambridge University Press
- Svanberg K (1987) The method of moving asymptotes - a new method for structural optimization. *International Journal for Numerical Methods in Engineering* 24:359–373
- Victoria M, Querin OM, Martí P (2011) Generation of strut-and-tie models by topology optimization using different material properties in tension and compression. *Structural and Multidisciplinary Optimization* 44:247–258
- Wang F, Lazarov BS, Sigmund O (2011) On projection methods, convergence and robust formulations in topology optimization. *Structural and Multidisciplinary Optimization* 43:767–784
- World Business Council for Sustainable Development (2012) The cement sustainability initiative: Executive brief. Tech. rep.
- Xu S, Cai Y, Cheng G (2010) Volume preserving nonlinear density filter based on heaviside functions. *Structural and Multidisciplinary Optimization* 41(4):495–505, DOI 10.1007/s00158-009-0452-7
- Yang Y, Moen CD, Guest JK (2014) Three-dimensional force flow paths and reinforcement design in concrete via stress-dependent truss-continuum topology optimization. *Journal of Engineering Mechanics* 141(1):04014,106
- Zhu J, Zhang W, Beckers P, Chen Y, Guo Z (2008) Simultaneous design of components layout and supporting structures using coupled shape and topology optimization technique. *Structural and Multidisciplinary Optimization* 36(1):29–41
- Zhu JH, Zhang WH, Xia L (2015) Topology optimization in aircraft and aerospace structures design. *Archives of Computational Methods in Engineering* pp 1–28



**Fig. 13** Setup for the optimization of a double-span simply supported beam subjected to a uniform load. Only the right symmetric half is presented.



**Fig. 14** The optimization evolution for a two-span beam, obtained with  $T_{pre} = 0.8 \times T_{STD}$ . From top to bottom: after 25, 50, 75, 100 and 200 design cycles.



**Fig. 15** The effect of self-weight on the optimization of a two-span beam. Top: without self-weight and  $T_{pre} = 0.8 \times T_{STD}$ ; Bottom: with dominant self weight and  $T_{pre} = 50 \times T_{STD}$ . When self-weight is dominant, material is more concentrated near the central support so that deformation due to self-weight is reduced.